Original Article

Proc IMechE Part F:
J Rail and Rapid Transit
2024, Vol. 238(10) 1296–1306

DOI: 10.1177/09544097241278761
journals.sagepub.com/home/pif

Mechanism and improvement for tail vehicle swaying of power-centralized EMUs

Yadong Song[1], Yuan Yao[1,2], Ming Lu[3] and Xing Wang[4]

Abstract

The swing phenomenon of the tail vehicle will reduce the stability of the train operation, and even seriously deteriorate the ride comfort of passengers. In response to the relevant railway department, this paper reported the different dynamics performances in tail vehicle swaying when power-concentrated EMUs passed through a tunnel under push/pull operation. To analyze the characteristics and mechanism of the EMU tail swaying, field tests and numerical simulations were conducted. Firstly, through the on-track test, it was found that under push operation, the EMU tail continued to sway at a frequency of 1.3 Hz inside the tunnel, while under pull operation, only a swing of 1.7 Hz appeared at the tunnel entrance. Subsequently, through a simulation analysis, it was found that under push operation, the vortex-induced vibration of the tail carbody occurred inside the tunnel, leading to the sustained swing with a carbody hunting frequency of 1.3 Hz; under pull operation, due to the aerodynamic effect of the tunnel entrance, the secondary lateral stop had an abnormal elastic collision with the bogie frame, and the lateral impact on the bottom of the tail carbody caused a swing of 1.7 Hz, which was verified by the field test. Finally, for the motor vehicle of the EMU tail, two improvement measures of yaw damper optimization were proposed to alleviate the EMU tail swaying inside the tunnel. Furthermore, the research results can provide a reference for the aerodynamic swing problem of other trains, which has certain engineering significance.

Keywords

Power-centralized EMU, push/pull operation, tail vehicle swaying, vehicle suspension improvement, field test

Date received: 2 April 2024; accepted: 4 August 2024

Introduction

Engineering background

In June 2022, the China Academy of Railway Sciences conducted a line test of the power-centralized EMUs (Electric Multiple Units) at the speed level of 160 km/h. The test results show that in the single-line tunnel, there is an obvious periodic swing at the train tail of the EMUs under both push and pull operations. Furthermore, the main frequency of tail vehicle swaying is in the range of 1–2 Hz, and the lateral Sperling index of the rear cab at the train tail can reach 3.4, which has attracted the attention of the relevant railway departments. Due to the strong aerodynamic effect in the single-line tunnel, it is judged that the swing phenomenon of the tail vehicle is caused by the airflow disturbance of the train wake.

The focus of this study is on the power-centralized EMUs that are operating on the Yu-Meng railway. The railway starts from Yuxi and ends in Mengzi, which is a key project for China to implement the western development strategy, and it is also an important part of the east line of the international railway channel (Trans-Asian Railway) in Yunnan Province. The total length of the line is around 150 km, of which bridges and tunnels account for about 55%, and there are many single-line tunnels.

Literature review

The phenomenon of train tail swaying inside tunnels can be traced back to the Japanese Shinkansen trains in the 1990s ,[1] and has gradually developed into a new research topic. The RTRI (Railway Technical Research Institute) of Japan, first conducted related research on it. Among them, Takai[2] found that the aerodynamic force inside tunnels is the main reason for the tail vehicle swaying, while the track excitation has little effect. Suzuki[3–5] analyzed the unsteady aerodynamic force acting on the train inside tunnels and regarded the phenomenon of train tail swaying as a forced vibration caused by the aerodynamic force. Furthermore, Fujimoto et al.[1] installed yaw dampers at the rear end of the train, which can effectively reduce the lateral vibration of the train tail on the Shinkansen line.

The train tail swing is mainly reflected in the low-frequency lateral swing of the tail carbody. In the vibration theory of railway vehicles,[6,7] the carbody low-frequency

[1]State Key Laboratory of Rail Transit Vehicle System, Southwest Jiaotong University, Chengdu, China
[2]State Key Laboratory of Heavy-duty and Express High-power Electric Locomotive, CRRC Zhuzhou Electric Locomotive Co., Ltd, Zhuzhou, China
[3]School of Railway, Shandong Polytechnic, Jinan, China
[4]School of Transportation Engineering, Dalian Jiaotong University, Dalian, China

Corresponding author:
Yuan Yao, State Key Laboratory of Rail Transit Vehicle System, Southwest Jiaotong University, No.111, North Section of Second Ring Road, Jinniu District, Chengdu 610031, China.
Email: yyuan8848@163.com

(within 1–2 Hz) swing belongs to the hunting motion of carbody hunting (i.e., primary hunting), and another high-frequency (higher than 5 Hz) hunting motion is the bogie hunting (i.e., secondary hunting). The carbody swing is mostly due to the vehicle's primary hunting instability, resulting in the low-frequency lateral vibration of the carbody with a large amplitude, which leads to the ride comfort deterioration or even derailment.[8] According to the existing experimental and simulation studies, improving wheel-rail contact conditions[9,10] and vehicle suspension optimization[7,11,12] are the two effective measures to solve the issue of carbody low-frequency swing.

As the train speed increases, the aerodynamic performance of the train has attracted more attention. The airflow around the train is a severe turbulence with significant unsteady characteristics. The safety assessment of train operation under crosswind has been widely studied.[13–15] However, few studies have examined the swing phenomenon of the train tail caused by train wake. Hemida et al.[16] found that when the train wake's vortex-shedding frequency is close to the carbody hunting frequency, the resonance will occur and aggravate the carbody vibration. Diedrichs et al.[17,18] compared the aerodynamic performance of the tail carbody of the Japanese S300 train and the German ICE2 train inside tunnels, and discovered that the vibration of the train tail was correlated with the shape and mass of the tail carbody. In references 19,20, the influence of aerodynamic forces on the vehicle's hunting stability of the high-speed train was analyzed. Chen et al.[21] proposed an innovative measure to improve the wheel-rail adhesion performance of high-speed trains by installing aerodynamic wings on the carbody.

Based on the fluid-structure coupling study of the train's aerodynamic performance inside tunnels, Ji et al.[22] found that the swing phenomenon of the high-speed train tail is the result of a combination of the aerodynamic effect and track excitation; Song et al.[23,24] found that the swing phenomenon of the 160 km/h EMU tail is due to the vortex-induced vibration (VIV) of the tail carbody under the aerodynamic effect of train wake.

Highlights of this paper

The paper describes the swing phenomenon of the power-centralized EMU tail under the push/pull operation inside the tunnel, and the highlights of this paper are as follows:

- The swing features of the EMU tail under the push and pull operations are presented respectively, and the corresponding swing frequencies are measured.
- The mechanism for the different dynamics performances in the EMU tail swaying under the push and pull operations is clarified, which is verified by the field test.
- From the perspective of the vehicle suspension improvement, two effective optimization measures of the yaw damper are proposed to alleviate the EMU tail swaying.

The rest of the paper is arranged as follows: In the next section, through the on-track test, the swing characteristics of the EMU tail under the push/pull operation inside single-line tunnels are investigated. In Section 3, through the numerical simulation, the mechanism for the difference in the EMU tail swaying under the two operations is illustrated. In Section 4, through the field test, the results of the simulation analysis in Section 3 are confirmed. In Section 5, countermeasures for the EMU tail swaying are put forward. Finally, some relevant conclusions are drawn in Section 6.

On-track test investigation

This section introduces the on-track test of the power-centralized EMU tail swaying in tunnels, which was carried out by our research team in November 2022, as shown in Figure 1. The operation route is the Yu-Meng railway line in Yunnan, China. The same EMUs were tested under the push and pull operations, respectively. Among them, when the EMUs operate under the push operation, the motor vehicle is at the EMU tail. While under the pull operation, the motor vehicle provides traction at the EMU head, and the EMU tail is the trailer vehicle.

In order to obtain the swing characteristics of the EMU tail, the vehicle measurement analyzer, supplied by China Chengdu Huaruizhichuang Rail Transit Technology Co., Ltd, was used to collect and analyze the vibration data of the train tail. The vibration sensor is mounted on the floor in the rear cab of the tail vehicle, as shown in Figure 1(b). In addition, the sampling frequency and range of the sensor are 1000 Hz and 2 g, respectively.

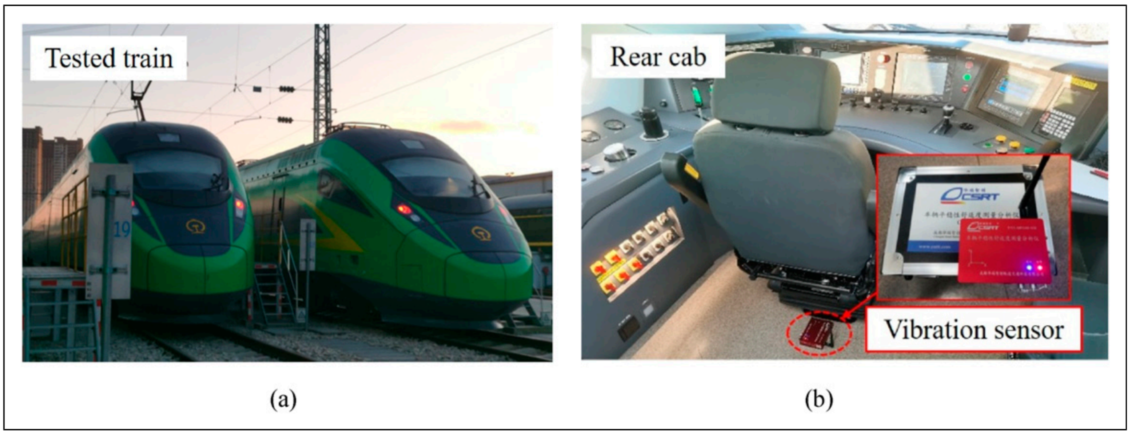

Figure 1. Tested power-centralized EMUs: (a) actual train; (b) sensor location.

According to our on-site riding experience, during every single-line tunnel condition, the EMU tail has a consistent swing performance, so the track excitation differences inside tunnels can be excluded. Therefore, we selected the typical long straight single-line tunnel of the railway, named Hanyi-Village Tunnel, and analyzed the dynamics performance of the tail vehicle passing through the tunnel. In addition, observing from the tachograph in the rear cab, the speed range of the EMU operating on this section was about 120–130 km/h.

Ride comfort evaluation

The vehicle ride comfort index is an essential indicator for evaluating carbody vibration and passenger comfort, which is calculated by the measurement of carbody vibration acceleration. The Sperling index is commonly used to evaluate the ride comfort of railway vehicles. According to the railway standard GB/T5599,[25] the lateral Sperling index W_y is defined as follows:

$$W_y = 3.57\left[\frac{A_y^{\,3}}{f}F(f)\right]^{1/10}. \tag{1}$$

where A_y is the amplitude from the FFT analysis of the measured carbody lateral acceleration (m/s^2), f is the corresponding vibration frequency (Hz), and $F(f)$ is the frequency-weighted parameter. In addition, the larger the value of W_y, the worse the lateral ride comfort. Moreover, the upper limit values for excellent lateral ride comfort of the trailer vehicle and the motor vehicle are 2.50 and 2.75, respectively.

Figure 2 shows the lateral ride index of the train tail when the EMUs pass through the Hanyi-Village Tunnel. It can be seen from Figure 2(a) that under the push operation, most lateral ride indices in the tunnel section are greater than the limit value of 2.75 and even up to 3.2, indicating that the continuous swing occurs after the train tail enters the tunnel. However, under the pull operation, the lateral ride index increases rapidly after entering the tunnel, which exceeds the limit value of 2.50, and then decreases slowly

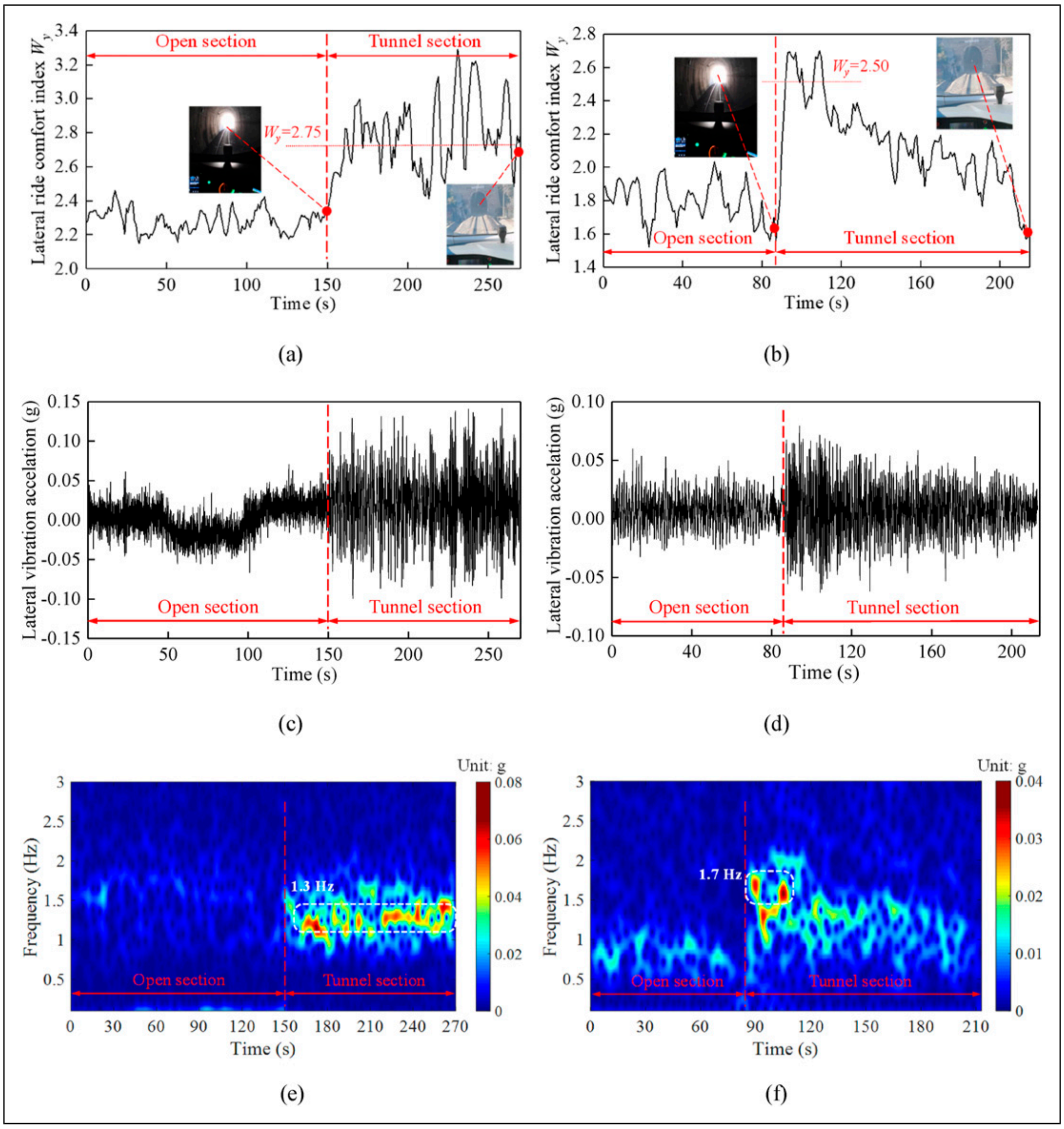

Figure 2. Test results of tail vehicles passing through the tunnel under push/pull operation: (a) lateral ride index of tail motor vehicle; (b) lateral ride index of tail trailer vehicle. (c) lateral acceleration in time-domain of tail motor vehicle; (d) lateral acceleration in time-domain of tail trailer vehicle. (e) lateral acceleration in frequency-domain of tail motor vehicle; (f) lateral acceleration in frequency-domain of tail trailer vehicle.

below 2.20, as shown in Figure 2(b), indicating that the train tail sways violently after entering the tunnel and then converges rapidly. These are completely consistent with the experimenter's feeling at the EMU tail under the push and pull operations.

Vibration characteristics analysis

To further research the swing characteristics of the EMU tail under the push and pull operations, the lateral acceleration of the train tail in the time-frequency domain is analyzed, as shown in Figure 2. Among them, Figure 2(e) and (f) are the short-time Fourier transform (STFT) results of Figure 2(c) and (d), respectively. Since the tail vehicle swaying belongs to the carbody low-frequency vibration, the visible range of the frequency axis is set to 0–3 Hz. In addition, according to the eigenvalue analysis results of the Simpack models below, at the speed of 130 km/h, the characteristic frequencies of the vehicle primary hunting mode (carbody hunting mode) of the motor vehicle and trailer vehicle are 1.3 Hz and 1.0 Hz, respectively.

It can be seen from Figure 2(e) that under the push operation, the train tail continues to swing at a frequency around 1.3 Hz in the tunnel, and 1.3 Hz is also the carbody hunting frequency, which has been described in detail in the author's previous research.[26–28] However, when the EMUs operate under the pull operation, the swing frequency of the train tail is around 1.7 Hz at the tunnel entrance, and then the swing phenomenon gradually disappears, as shown in Figure 2(f).

Furthermore, the sensitive frequency range of the human body to horizontal vibration is around 1–2 Hz, which means passengers will feel obvious discomfort in this frequency range, and the human body will not feel the vibration difference between 1.3 Hz and 1.7 Hz. To clarify the mechanism for the difference in the EMU tail swaying under the push and pull operations inside single-line tunnels, the numerical simulation is carried out in the next section.

Numerical simulations

Technical route

In this paper, the numerical calculation method of fluid-structure coupling is used to simulate the vortex-induced vibration of the tail carbody, and the co-simulation model and method have been introduced in detail in the author's previous research.[23]

As shown in Figure 3, the train multi-body dynamics model and train aerodynamics model under two conditions of push and pull operations are established, respectively. The phenomenon of EMU tail swaying is mainly reflected in the lateral motion y, rolling motion α, and yawing motion γ of the tail carbody. Therefore, the multi-body dynamics model transfers the three motion states of the tail carbody to the aerodynamics model, and the aerodynamics model transfers the aerodynamic load of the tail carbody to the multi-body dynamics model to complete the co-simulation simulation. The time step Δt of data exchange is set to 0.005 ms, and the total simulation time $n{\cdot}\Delta t$ is set to 10 s.

Dynamic modeling

Train multi-body dynamics model. The multi-body dynamics model of the power-centralized EMU is developed in the software SIMULIA Simpack 2020, and the EMU model consists of six vehicles. The main dynamics parameters of the motor vehicle and the trailer vehicle are illustrated in Table 1.

For the Simpack model of the trailer vehicle, it consists of 17 rigid bodies with 54 degrees of freedom. For the Simpack model of the motor vehicle, there are four more pairs of traction motors and hollow shafts, which consist of 25 rigid bodies and have 90 degrees of freedom. The specific modeling and accuracy of the Simpack models have been described in the author's previous research.[26–28]

The main differences between the dynamic models of the motor vehicle and the trailer vehicle are as follows: The motor vehicle has four more traction motors, as shown in Figure 4(a), so the axle load is much larger than the trailer vehicle; the trailer vehicle adopts the softer secondary suspension of air spring, which can better reduce the wheel-rail impact to the carbody, as shown in Figure 4(b). In addition, significant differences also exist in the secondary suspension parameters, as shown in Table 1.

Train aerodynamics model. The vortex-induced force acting on the EMU tail inside a single-line tunnel is simulated by the commercial software SIMULIA Xflow 2021x. The train aerodynamic model of six vehicles is established, and the vehicle is simplified according to the CEN standard.[29,30] Moreover, the vehicle is composed of a simplified carbody and bogie, without considering the details of the pantograph, window, and door. For the aerodynamic shape of the tail carbody, the nose shape of the motor vehicle and the trailer motor are the same, but the length of the motor vehicle is longer, as shown in Figure 4. The carbody height H of the EMU is 4.0 m, and the shape of the single-line tunnel refers to the standard GB 146.2,[31] as shown in Figure 4(d). In addition, the specific settings of the train aerodynamic model, including the computational domain, boundary conditions, grid independence, etc., have been described in the author's recent research.[23]

Simulation conditions

In the co-simulation, the speed of the EMUs operating in the tunnel is 130 km/h, corresponding to the actual speed of the on-track test in Section 2 above. In addition, the track irregularity has been described in detail in the author's previous research.[23] Two simulation conditions of push and pull operations are set up, corresponding to Condition 1 and Condition 2, respectively, as follows:

Condition 1. push operation, with tail motor vehicle;
Condition 2. pull operation, with tail trailer vehicle.

Unfortunately, the vortex-induced vibration coupling model introduced in this paper only simulates the aerodynamic characteristics of the train operating inside tunnels, without considering the aerodynamic effect of the tunnel entrance. However, the amplitude of aerodynamic force at

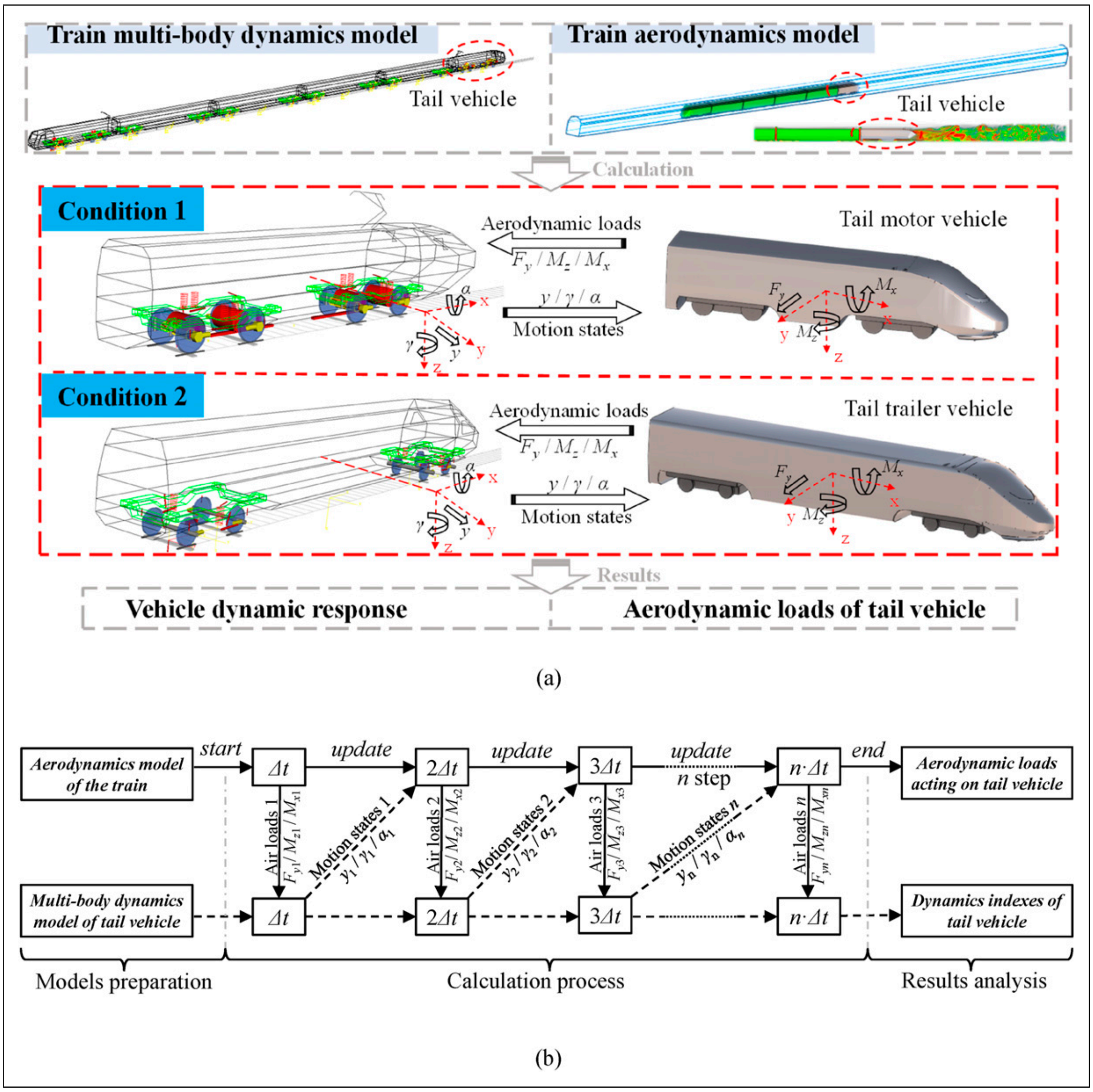

Figure 3. Method of simulation: (a) co-simulation models; (b) workflow of coupling calculation.

Table 1. Dynamics parameters of the motor/trailer vehicle.

Item	Value	Unit
Mass of carbody	42907	kg
Mass of bogie frame	3442/2210	kg
Mass of wheelset	2434/1445	kg
Mass of traction motor	2359/−9/18	kg
Length between bogies	2900/2600	m
Bogie wheelbase	1250/915	mm
Wheel diameter	25/30	mm
Damping of secondary lateral damper	8.5/25	kN·s/m
Series stiffness of secondary lateral damper	800/200	kN/mm
Yaw damper damping	22.5	kN·s/m
Series stiffness of yaw damper	35/20	kN/mm
Gap of secondary lateral stop	JM3/LM	mm
Wheel tread	CN60	—
Rail profile	1:40	—
Rail cant	0.11/0.10	—
Wheel/rail contact equivalent conicity		—

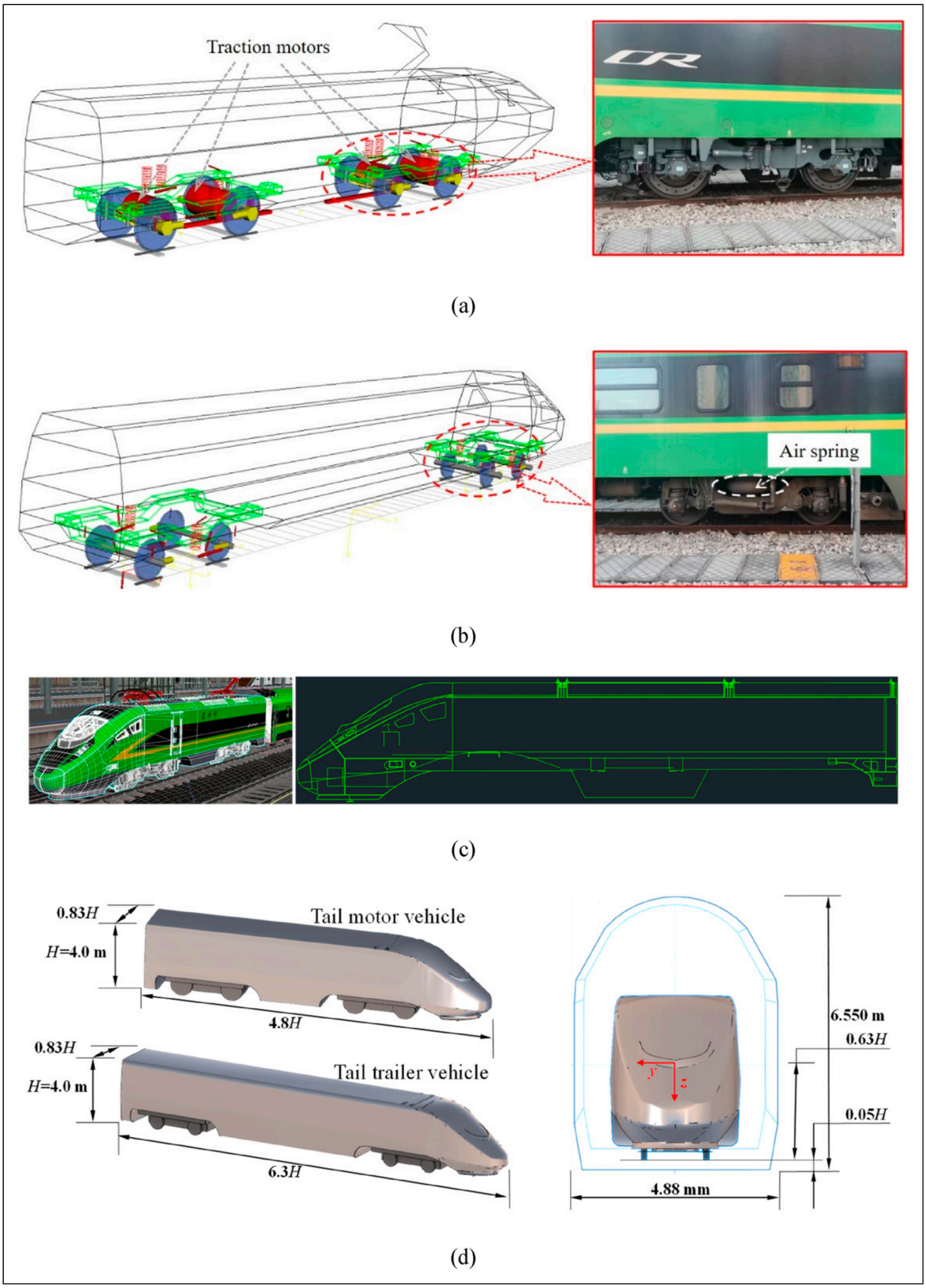

Figure 4. Schematic diagrams of train model: (a) multi-body dynamics model of motor vehicle; (b) multi-body dynamics model of trailer vehicle. (c) actual shape of tail vehicle; (d) aerodynamics shape of simplified vehicles.

the tunnel entrance is about twice larger than that inside tunnels.[22] According to the swing characteristics of the tail trailer vehicle, it is conjectured that the tail vehicle swaying under the pull operation is caused by the aerodynamic impact of the tunnel entrance. Therefore, for Condition 2, in the first 3 s of the coupling calculation, the aerodynamic force is doubled to represent the aerodynamic impact at the tunnel entrance.

Result analysis

According to the author's recent research,[23] the aerodynamic loads M_x, M_z, and F_y acting on the tail carbody are caused by the excitation of the train wake, and the time-frequency variation of aerodynamic loads is determined by the vortex-shedding effect of the train wake. Moreover the aerodynamic pressure acting on the carbody surface generates the aerodynamic force F_y on the carbody, thus generating the aerodynamic torques M_x and M_z. Hence, only the typical vortex-induced force F_y is analyzed here, and M_x, M_z are omitted.

In addition, the two primary factors influencing the dynamic characteristics of the vortex-induced force F_y are the train speed and tail-nose shape.[23] Due to the unsteady characteristics of the train wake, for the transient calculation of the vortex-induced force in this paper, it is considered that if the amplitude and dominant frequency of the vortex-induced force correspond to the same respectively, the variation of the vortex-induced force acting on the tail carbody is nearly the same. The results of vortex-induced force F_y acting on the tail carbody under the push and pull operations are shown in Figure 5(a) and (b), respectively. It can be seen that inside the tunnel, at the same operating speed, due to the identical nose shapes of the tail motor vehicle and the tail trailer vehicle, the variation of the vortex-induced force acting on the tail carbody is nearly the same, The lateral acceleration of the train tail under the push and pull operations is shown in Figure 5(c) and (d), respectively, and the corresponding lateral ride indices W_y are shown in Table 2, which is almost consistent with the test results in Figure 2(a) and (b). It can be seen that inside the tunnel, the vortex-induced force leads to the sustained swing of the tail motor vehicle due to vortex-induced vibration,[23] while the vortex-induced force inside tunnels has little effect on the lateral ride comfort of the tail trailer vehicle, because the primary hunting stability of the trailer vehicle is better due to its own vehicle suspension structure.

Next, to clarify the abnormal swing phenomenon of the tail trailer vehicle at the tunnel entrance, the dynamic response of its secondary lateral stop is analyzed. As illustrated in Table 1, the design gap of the secondary lateral stop for the trailer vehicle is 20 mm, which is much smaller than that of the motor vehicle with 35 mm, thus there is a possibility of the collision for the tail trailer vehicle's secondary lateral stop under the aerodynamic impact.

The secondary lateral stop is an elastic buffer device installed between the carbody and the bogie frame to limit the excessive lateral movement of the carbody. According to the handbook of railway vehicle dynamics,[32] when running on a straight line, the stop should not contact the frame; when passing through a curved line, especially a sharp-radius curve, in order to ensure the safety of curve passing, the stop should contact the frame. Meanwhile, the suitable gap of the secondary lateral stop is an important factor to ensure the good performance of curve passing.

Figure 5(f) shows the lateral movement of the secondary lateral stop near the train tail under the pull operation, and the green dashed line represents the critical value of the collision between the secondary lateral stop and the bogie frame, which means that the elastic collision occurs when the lateral movement of the stop exceeds 20 mm. At the tunnel entrance, the rear lateral stop of the tail trailer vehicle collides with the frame, causing a lateral impact on the bottom of the tail carbody, as shown in Figure 5(h). For the rear lateral stop of the tail motor vehicle, the gap of the lateral stop is relatively large at 35 mm, and the collision will not happen inside the tunnel, as shown in Figure 5(e) and (g).

It can be concluded that under the push operation, vortex-induced vibration of the tail carbody occurs inside the tunnel, presenting a swing frequency of carbody hunting at 1.3 Hz; under the pull operation, due to the aerodynamic effect of the tunnel entrance, the secondary lateral stop near the train tail has an abnormal collision with the bogie frame, which has a lateral impact on the bottom of the tail carbody at the tunnel entrance, presenting a swing frequency of the carbody impact at 1.7 Hz.

Field test validation

In this section, the simulation results of Condition 2 above are verified by field tests, as shown in Figure 6. For the actual operation of the tail motor vehicle, the gap of the lateral stop is small, and its bogie structure is complex (with motor suspension). Due to the limited space, it is difficult to achieve the installation of sensors, so this method of marking is adopted. The right and left positions of the frame that may collide with the secondary lateral stop near the train tail, are painted with red marks, as shown in subgraphs 1 and 3 of Figure 6(b), respectively. The subgraphs 2 and 4 of Figure 6(b) are the test results of the EMUs passing through the Hanyi-Village Tunnel under the pull operation. For the tested straight tunnel track without turnout, the secondary lateral stop should not contact with the frame, only under the aerodynamic impact of the tunnel, the abnormal collision mark between the frame and the secondary lateral stop may occur.

It can be seen that when the EMUs passed through the long straight single-line tunnel, the abnormal collision between the lateral stop and the frame occurred. Therefore, it is verified that when the EMUs passed through the tunnel under the pull operation, the aerodynamic impact of the tunnel entrance caused the abnormal elastic collision between the lateral stop and the bogie frame, which may lead to the coupling mode of the yaw motion and the rolling motion of the tail carbody, resulting in a 1.7 Hz swing phenomenon of the EMU tail.

Improvement for tail motor vehicle

The issue of the EMU tail swaying in the tunnel under the push operation is much more serious than that under the pull operation. Therefore, in this section, aiming at the tail motor vehicle of Condition 2 as illustrated in Section 3 above, we put forward two improvement measures of yaw damper optimization to alleviate the train tail swaying without changing the vehicle structure.

For the motor vehicle in this paper, there is a contradiction in the impact of C_{sx} on the dynamic performance,[27,28] reducing C_{sx} is beneficial to increase the carbody hunting stability, while increasing C_{sx} is beneficial to increase the bogie hunting stability. Moreover, in the theory of railway vehicle suspension,[7,32] the carbody low-frequency swing is due to the instability of primary hunting (i.e., carbody hunting), and reducing the secondary suspension damping within a certain range can improve the carbody hunting stability. Consequently, Countermeasure 1 is put forward to reduce the damping C_{sx} of the yaw damper from the initial 800 kN·s/m to 600 kN·s/m.

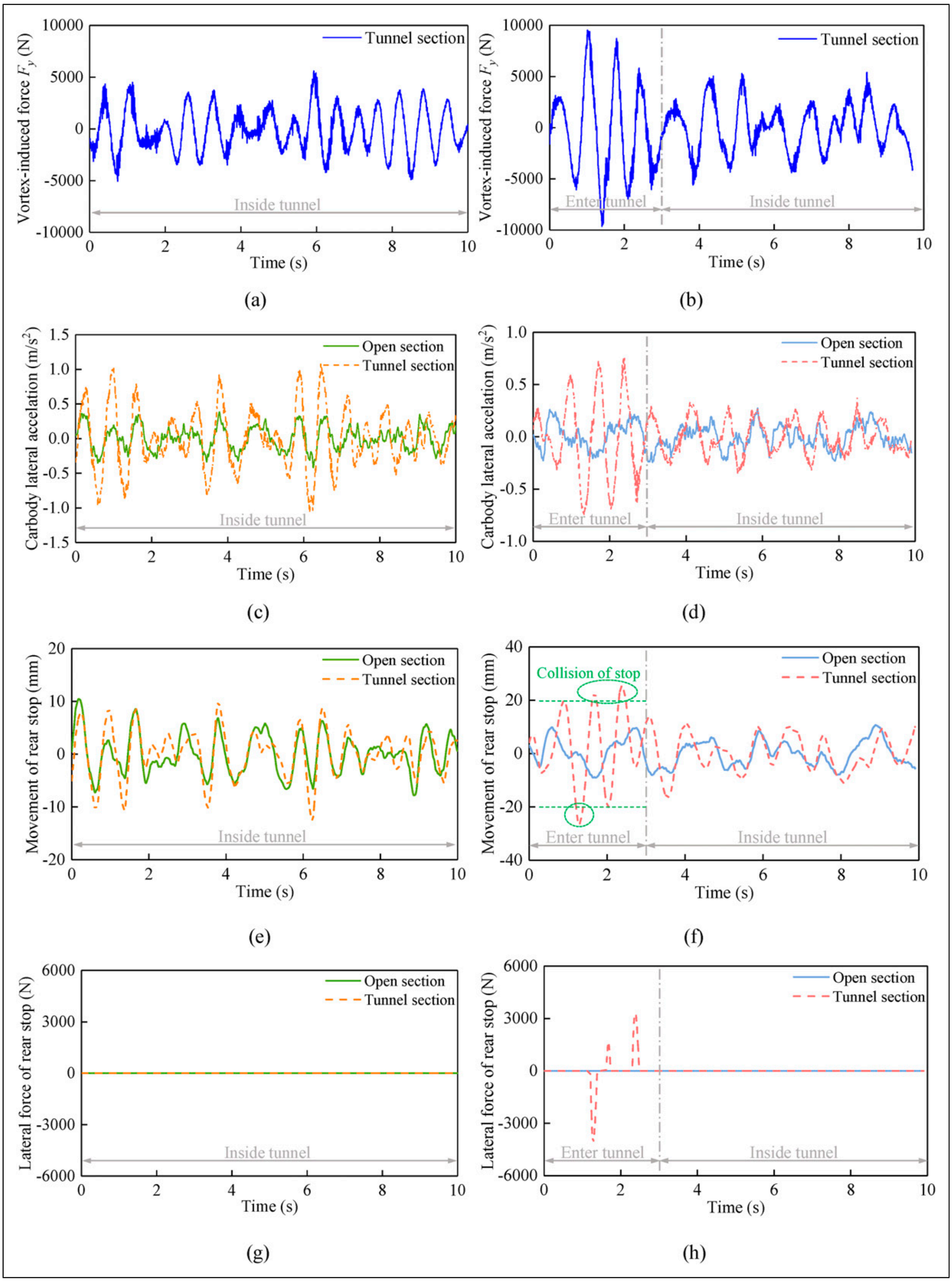

Figure 5. Simulation results of vehicle dynamic responses under push/pull operation: (a) tail carbody's aerodynamic force of Condition 1; (b) tail carbody's aerodynamic force of Condition 2; (c) tail carbody's acceleration of Condition 1; (d) tail carbody's acceleration of Condition 2; (e) rear stop's lateral movement of Condition 1; (f) rear stop's lateral movement of Condition 2; (g) rear stop's lateral force of Condition 1; (h) rear stop's lateral force of Condition 2.

In general, the layout of yaw dampers for railway vehicles is mainly divided into two types: skew symmetry (SS) and opening outward (OO), as shown in Figure 7. The motor vehicle of the power-centralized EMUs adopts the yaw damper of the SS layout. There is no doubt that the SS layout is beneficial to the vehicle's dynamics performance in some aspects, but it will also lead to a contradiction in lateral ride comfort of the carbody's rear and front ends.[26] Consequently, the Countermeasure 2 is put forward, with yaw dampers of the OO layout.

The lateral dynamics performances of the tail motor vehicle under the two countermeasures are shown in Table 3, which is the calculation result of the Simpack model for the motor vehicle in Figure 4(a) in Section 3.2 above. Moreover, the "Front-end" is the leading edge of tail carbody, and the "Rear-end" is the rear edge of the carbody. Under the push operation of the EMUs, for the tail motor vehicle, the backward force (coupler force) will reduce the lateral stability of the rear-end of the carbody to a certain extent. As shown in Table 3, the W_y of the front-end of the carbody is 2.08, and the W_y of the rear-end of the carbody is 2.34 under the initial suspension parameters. However, the backward force is not the main factor affecting the EMU tail swaying, and the

Table 2. Lateral ride comfort of the train tail under push/pull operation.

		Single-track tunnel section	
Lateral ride comfort index W_y	Open section	Enter tunnel	Inside tunnel
Condition 1	2.34	-	2.96
Condition 2	1.92	2.78	2.06

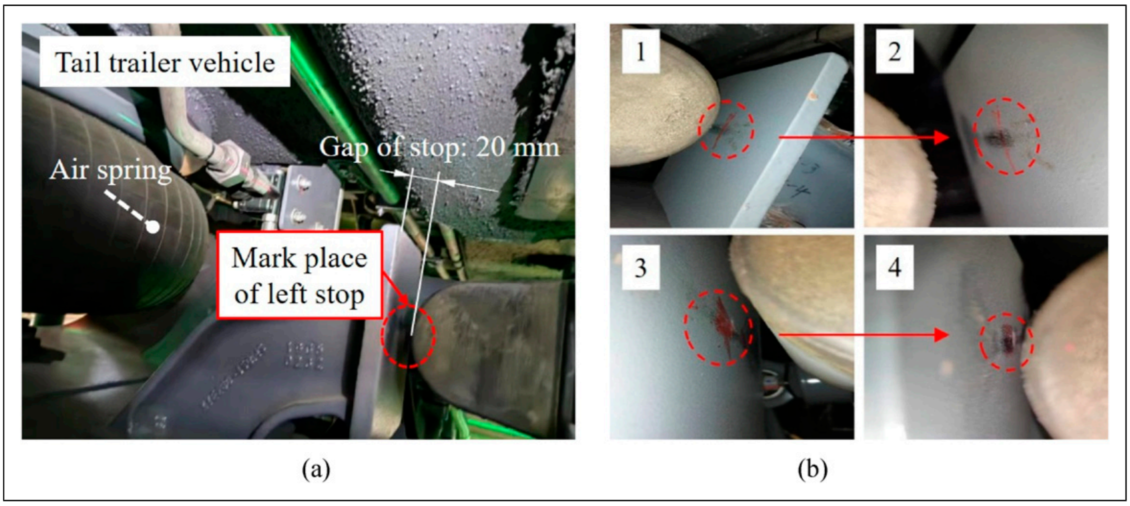

Figure 6. Measurement of secondary lateral stop: (a) mark location; (b) test photos.

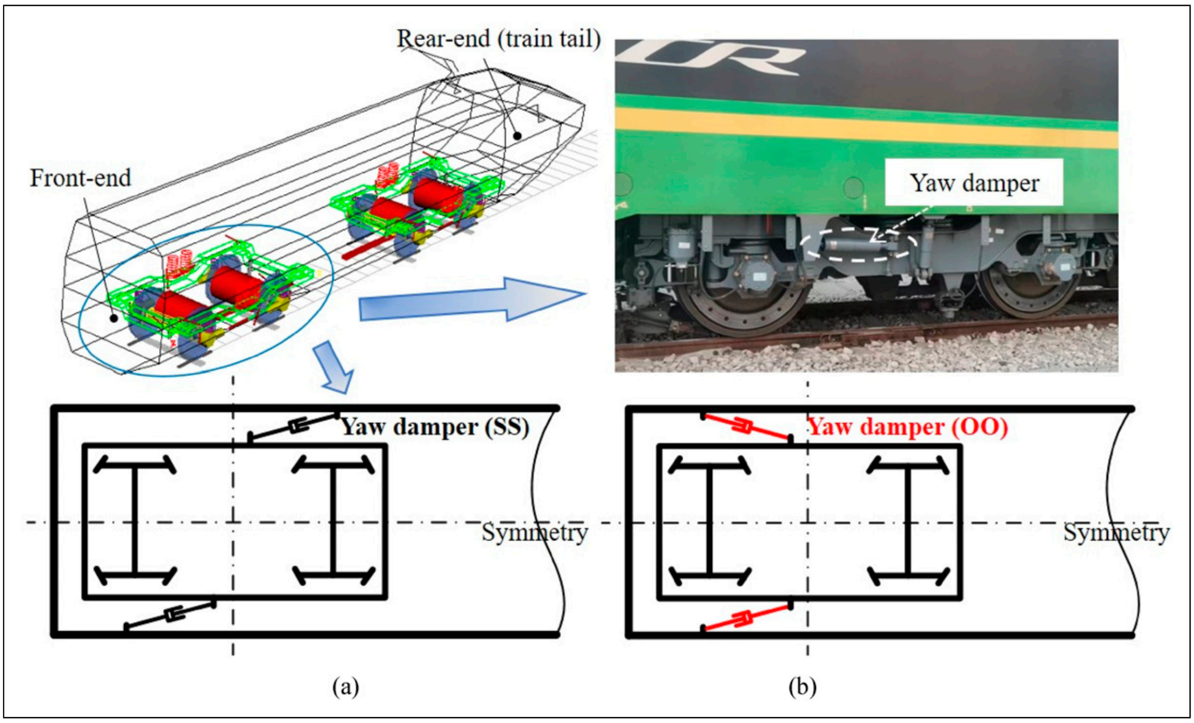

Figure 7. The layout of yaw dampers: (a) initial; (b) countermeasure 2.

Table 3. Lateral ride comfort of the tail motor vehicle (open section/tunnel section).

Vehicle suspension	Yaw damper arrangement	Yaw damper damping C_{sx} (kN·s/m)	Lateral comfort index W_y	
			Front-end	Rear-end
Initial	SS	800	2.08/2.13	2.34/2.96
Countermeasure 1	SS	600	2.05/2.11	2.26/2.74
Countermeasure 2	OO	800	2.14/2.17	2.15/2.72

aerodynamic vortex-induced force inside the tunnel is the main factor.

It can be seen that the W_y of the EMU tail (carbody's rear-end) is 2.34 during the open section, while the W_y of the EMU tail deteriorates to 2.96 during the tunnel section (with vortex-induced force), which is almost consistent with the on-track test results in Figure 2(a). Furthermore, under Countermeasures 1 and 2, the lateral ride index W_y of the EMU tail is 2.74 and 2.72, respectively, both of which are at the excellent level (less than 2.75), indicating that the two suspension improvement measures can effectively alleviate the swing phenomenon of the tail motor vehicle inside the tunnel.

Conclusion and outlook

In this paper, based on the power-centralized EMUs operating on the Yu-Meng railway, the different dynamics performances of the tail vehicle swaying under the push/pull operation inside tunnels are analyzed by field tests and numerical simulations, and two suspension measures to alleviate the tail motor vehicle swaying are proposed. The relevant conclusions are as follows:

(1) At the same operating speed, due to the identical nose shapes of the tail motor vehicle and the tail trailer vehicle, the vortex-induced force acting on the EMU tail is nearly the same under both push and pull operations inside tunnels. Meanwhile, the difference in the EMU tail swaying is determined by the suspension structure of the tail vehicle under the two operations.
(2) Under the push operation, due to the vortex-induced vibration of the tail carbody inside the tunnel, the tail motor vehicle continues to sway with the primary hunting frequency of 1.3 Hz;
(3) Under the pull operation, due to the aerodynamic effect of the tunnel entrance, the secondary lateral stop of the tail vehicle has an abnormal elastic collision with the bogie frame, and the lateral impact on the bottom of the tail carbody causes a swing of 1.7 Hz at the tunnel entrance.
(4) For the motor vehicle of the EMU tail, employing the yaw damper of the opening outward (OO) layout or decreasing the yaw damper damping within a set range to improve its primary hunting stability can effectively alleviate the EMU tail swaying inside the tunnel.

In future work, the aerodynamic shape optimization of the tail carbody will be conducted to weaken the EMU tail swaying, and the aerodynamic simulation of the tunnel entrance will also be refined.

Declaration of conflicting interests

The author(s) declared no potential conflicts of interest with respect to the research, authorship, and/or publication of this article.

Funding

The author(s) disclosed receipt of the following financial support for the research, authorship, and/or publication of this article: The material in this paper is based on work supported by National Natural Science Foundation grant of China (52372403, U2268211), Sichuan Natural Science Foundation grant (2022NSFSC0034, 2022NSFSC1901), and National Railway Group Science and Technology Program grant (N2023J071).

ORCID iD

Yuan Yao https://orcid.org/0000-0003-2279-7463

References

1. Fujimoto H, Miyamoto M and Shimamoto Y. Lateral vibration and its decreasing measure in the tail car of a shinkansen. Decrease of tail car's vibration with yaw damper between cars. *Trans JSME Ser C* 1993; 59(560): 1016–1022.
2. Takai H. Maintenance of track with long-wave track irregularity on Shinkansen. *QR of RTRI* 1990; 3: 13–20.
3. Suzuki M. Unsteady aerodynamic force acting on high speed trains in tunnel. *QR of RTRI* 2001; 42(2): 89–93.
4. Suzuki M. Aerodynamic force acting on train in tunnel. *RTRI Report* 2000; 14(9): 37–42, [In Japanese].
5. Suzuki M. Flow-induced vibration of high-speed trains in tunnels. *Lect Notes Appl Comput Mesh* 2004; 19: 443–452.
6. Chen XW, Yao Y, Shen LJ, et al. Multi-objective optimization of high-speed train suspension parameters for improving hunting stability. *Int J Rai Transp* 2022; 10(2): 159–176.
7. Li YX, Chi M, Guo ZT, et al. An abnormal carbody swaying of intercity EMU train caused by low wheel-rail equivalent conicity and damping force unloading of yaw damper. *Rai Eng Sci* 2023; 31(3): 252–268.
8. Sun JF, Chi MR, Cai WB, et al. An investigation into evaluation methods for ride comfort of railway vehicles in the case of carbody hunting instability. *Proc IMechE Part F: J Rai Rapid Transit* 2021; 235(5): 586–597.
9. Li W, Guan QH, Chi MR, et al. An investigation into the influence of wheel-rail contact relationships on the carbody hunting stability of an electric locomotive. *Proc IMechE Part F: J Rai Rapid Transit* 2022; 236(10): 1198–1209.
10. Wu Y, Zeng J, Qu S, et al. Low-Frequency carbody sway modelling based on low wheel-rail contact conicity analysis. *Shock Vib* 2020; 2020: 1–17. DOI: 10.1155/2020/6671049.

11. Huang CH, Zeng J and Liang SL. Carbody hunting investigation of a high speed passenger car. *J Mech Sci Technol* 2013; 27(8): 2283–2292.
12. Sun JF, Chi MR, Jin XS, et al. Experimental and numerical study on carbody hunting of electric locomotive induced by low wheel-rail contact conicity. *Veh Syst Dyn* 2021; 59(2): 203–223.
13. Li T, Zhang JY and Zhang WH. A numerical approach to the interaction between airflow and a high-speed train subjected to crosswind. *J Zhejiang Univ A* 2013; 14(7): 482–493.
14. Liu Y, Han Y, Li CG, et al. Aerodynamic characteristics and dynamic performance of the moving train under crosswind. *Int J Struct Stabil Dynam* 2023; 23(11): 2350121.
15. Yao ZY, Zhang N, Zhu MC, et al. Dynamic interaction analysis and running safety assessment of the wind-train-bridge system considering the moving train's aerodynamic coupling with crosswind. *Int J Struct Stabil Dynam* 2023; 23(15): 2350173.
16. Hemida H and Krajnovic S. Exploring flow structures around a simplified ICE2 train subjected to A 30° side wind using LES. *Eng Appl Comp Fluid Mech* 2009; 3(1): 28–41.
17. Diedrichs B, Berg M, Stichel S, et al. Vehicle dynamics of a high-speed passenger car due to aerodynamics inside tunnels. *Proc IMechE Part F: J Rai Rapid Transit* 2007; 221(4): 527–545.
18. Diedrichs B, Krajnović S and Berg M. On the aerodynamics of car body vibrations of high-speed trains cruising inside tunnels. *Eng Appl Comp Fluid Mech* 2008; 2(1): 51–75.
19. Zeng XH, Lai J and Wu H. Hunting stability of high-speed railway vehicles under steady aerodynamic loads. *Int J Struct Stabil Dynam* 2018; 18(7): 1850093.
20. Wang JC, Ling L, Ding X, et al. The influence of aerodynamic loads on carbody low-frequency hunting of high-speed trains. *Int J Struct Stabil Dynam* 2022; 22(13): 2250145.
21. Chen Y, Jing L, Li T, et al. Numerical study of wheel–rail adhesion performance of new-concept high-speed trains with aerodynamic wings. *J Zhejiang Univ A* 2023; 24(8): 673–691.
22. Ji ZL, Liu W, Guo DL, et al. Analysis of the fluid–structure coupling characteristics of a high-speed train passing through a tunnel. *Int J Struct Stabil Dynam* 2022; 22(16): 2250185.
23. Song YD, Qin T, Yao Yet al. Investigation on aerodynamic fluid-structure coupling vibration of 160 km/h EMU tail in single-track tunnels. *Int J Struct Stabil Dynam*. 2023; 2450197.. doi:10.1142/S0219455424501979.
24. Yao Y, Xu G, Song YD, et al. Mechanism of train tail lateral sway of EMUs in tunnel based on vortex-induced vibration. *J Traffic Transport Eng* 2021; 21(5): 51–61, [in Chinese].
25. National Railway Administration. *GB/T5599. Specification for dynamics performance assessment and testing verification of rolling stock*. Beijing, China: National Railway Administration, 2019. [in Chinese].
26. Li G, Yao Y, Shen LJ, et al. Influence of yaw damper layouts on locomotive lateral dynamics performance: pareto optimization and parameter analysis. *J Zhejiang Univ A* 2023; 24(5): 450–464.
27. Li G, Wu RD, Deng XX, et al. Suspension parameters matching of high-speed locomotive based on stability/comfort Pareto optimization. *Veh Syst Dyn* 2022; 60(11): 3848–3867.
28. Li G, Zhou Y, Yuan Y, et al. Application of yaw dampers with frequency-selective damping to improve the locomotive adaptability to low/high conicity stability. *Proc IMechE Part F: J Rai Rapid Transit* 2022; 237(6): 784–795.
29. CEN European Standard. *Railway applications-aerodynamics. Part 4: requirements and test procedures for aerodynamics on open track*. Europe: CEN, 2009, vol EN 14067-4.
30. CEN European Standard. *Railway applications-aerodynamics. Part 6: requirements and test procedures for cross wind assessment*. Europe: CEN, 2010, vol EN 14067-6.
31. *GB 146.2-2020 Gauge for standard gauge railways Part 2: structure gauge*. [in Chinese].
32. Iwnicki S, Spiryagin M, Cole C, et al. *Handbook of railway vehicle dynamics*. 2nd ed. Boca Raton (FL): CRC Press, 2020.